Research Square

Preprints are preliminary reports that have not undergone peer review.
They should not be considered conclusive, used to inform clinical practice,
or referenced by the media as validated information.

c-Myc promotes pulmonary fibrosis by driving myofibroblast activation and cellular senescence

Xiaomin Peng
First Affiliated Hospital of Guangzhou Medical University
Yuqi Mai
First Affiliated Hospital of Guangzhou Medical University
Ruijuan Guan
First Affiliated Hospital of Guangzhou Medical University
Hang Yin
First Affiliated Hospital of Guangzhou Medical University
Yinuo Wang
First Affiliated Hospital of Guangzhou Medical University
Hailin Liao
First Affiliated Hospital of Guangzhou Medical University
Jin Yu
First Affiliated Hospital of Guangzhou Medical University
Penghui Yang
First Affiliated Hospital of Guangzhou Medical University
Xu Chen
cxdreamsky@163.com

First Affiliated Hospital of Guangzhou Medical University

Research Article

Keywords: Idiopathic pulmonary fibrosis, c-Myc, Cellular senescence, Myofibroblasts, TGF-beta1

Posted Date: July 12th, 2026

DOI: https://doi.org/10.21203/rs.3.rs-10232185/v1

License: This work is licensed under a Creative Commons Attribution 4.0 International License.
Read Full License

Additional Declarations: No competing interests reported.

Abstract

Background

Idiopathic pulmonary fibrosis (IPF) is a devastating and progressive interstitial lung disease characterized by aberrant myofibroblast activation, cellular senescence, and excessive extracellular matrix (ECM) deposition. However, the precise molecular switches governing these pathogenic processes in lung fibroblasts remain incompletely understood. Although the transcription factor c-Myc has been implicated in various organ fibroses, its specific role and underlying mechanisms in pulmonary fibrosis remain largely unexplored. Here, we investigated the pathogenic role of c-Myc in IPF fibroblasts and bleomycin (BLM)-induced pulmonary fibrosis.

Methods

Single-cell RNA sequencing (scRNA-seq) datasets and clinical human lung tissues from IPF patients and healthy donors were analyzed to evaluate c-Myc expression patterns. *In vivo*, C57BL/6 mice were intratracheally administered an adeno-associated virus serotype 9 (AAV9) vector to overexpress c-Myc prior to BLM injury. Lung damage was evaluated using Micro-CT and histopathological analysis. *In vitro*, primary human IPF fibroblasts were transduced with lentiviral vectors for c-Myc overexpression or short hairpin RNA (shRNA)-mediated knockdown. Fibroblast activation, proliferation, migration, and senescence were assessed using RT-qPCR, Western blotting, EdU incorporation, wound-healing, transwell assays, and SA-β-gal staining. Transcriptomic alterations following c-Myc depletion were further evaluated via RNA-seq.

Results

scRNA-seq analysis and clinical validations revealed that c-Myc is substantially upregulated in IPF lungs and predominantly enriched in the fibroblast population. *In vitro*, lentiviral overexpression of c-Myc exacerbated TGF-β1-induced myofibroblast activation, hyperproliferation, migration, and ECM production. Conversely, targeted c-Myc knockdown effectively abolished these profibrotic behaviors and profoundly suppressed the cellular senescence phenotype, characterized by decreased expression of p16, p21, and p53. Mechanistically, c-Myc deficiency blocked the canonical TGF-β1/Smad2/3 signaling cascade, and RNA-seq profiling confirmed the systemic blunting of proliferation, senescence, and ECM-producing gene networks. *In vivo*, AAV9-mediated c-Myc overexpression significantly aggravated BLM-induced lung consolidation and structural distortion in mice.

Conclusions

c-Myc is significantly upregulated in IPF and functions as a critical pathogenic driver that orchestrates myofibroblast activation and cellular senescence through the TGF-β1/Smad signaling pathway. Targeted inhibition of c-Myc effectively uncouples these profibrotic responses, suggesting that the c-Myc signaling axis represents a promising translational therapeutic target for idiopathic pulmonary fibrosis.

1. Introduction

Idiopathic pulmonary fibrosis (IPF) is a chronic, progressive fibrosing interstitial lung disease of unknown cause and is defined by a usual interstitial pneumonia pattern in the appropriate clinical context [1, 2]. Each year around 40,000 new cases of IPF are diagnosed in Europe alone [3]. The disease is associated with progressive loss of lung function, respiratory failure and a median survival of only 3–5 years after diagnosis [4, 5]. With the population aging worldwide, the incidence and economic burden of IPF are expected to steadily increase in the future [4]. Approved anti-fibrotic drugs (pirfenidone, nintedanib and the recently approved nerandomilast) can slow decline in lung function and reduce the risk of acute respiratory deteriorations; however, they do not offer a cure and are also associated with tolerability issues [6, 7]. Thus, novel therapeutic approaches are urgently needed.

Pathologically, IPF is sustained by repeated alveolar epithelial injury and aberrant repair, which promote the recruitment, expansion and activation of fibroblasts [8]. Ample evidence demonstrates that a defining feature of IPF is the activation and unremitting presence of myofibroblasts in “fibroblastic foci” (the leading edge of active fibrosis) of the IPF lungs [9, 10]. Myofibroblasts are characterized by *de novo* expression of α-smooth muscle actin (α-SMA), formation of stress fibers, and increased capacity to migrate, contract, and synthesize the extracellular matrix (ECM), which results in distortion of normal lung structures and loss of respiratory function [11–13]. In this process, transforming growth factor-β1 (TGF-β1) acts as the key pro-fibrotic cytokine that induces fibroblast recruitment, proliferation and differentiation into myofibroblasts [14]. TGF-β1 first binds to TGF-β receptor type II (TβRII), which then recruits, heterodimerizes with and phosphorylates TGF-β receptor type I (TβRI) to form an active ligand–receptor complex. This TGF-β–TβRII/I complex initiates pro-fibrotic responses by inducing fibroblast activation and differentiation through both canonical and non-canonical signaling pathways [8]. Hence, targeting TGF-β1 signaling represents a potential therapeutic strategy in the treatment of IPF.

Cellular senescence, an evolutionarily conserved state of stable cell cycle arrest, is increasingly recognized as a critical driving mechanism in the pathogenesis of IPF [15, 16]. Emerging evidence has demonstrated that fibroblasts within IPF lungs exhibit a prominent senescent phenotype. This state is characterized by elevated reactive oxygen species (ROS) production, persistent DNA damage, high activity of senescence-associated β-galactosidase (SA-β-gal), and the upregulation of key cell cycle repressors, including p53, p21, and p16 [17–20]. Rather than being a passive endpoint, fibroblast senescence can reinforce myofibroblast differentiation and ECM deposition [17–19]. Furthermore, senescent cells often acquire a senescence-associated secretory phenotype (SASP), releasing a myriad of pro-fibrotic cytokines that amplify tissue remodeling and propagate a vicious cycle of persistent fibrosis [16, 21]. Indeed, the targeted elimination of senescent cells—either genetically or

pharmacologically—has been shown to effectively alleviate pulmonary fibrosis and improve lung function in experimental models [22–24]. These observations suggest that the regulatory nodes connecting profibrotic signaling, fibroblast senescence and matrix remodeling may represent important disease-modifying targets.

c-Myc, encoded by proto-oncogene *MYC*, is a pleiotropic transcription factor that regulates cell growth, proliferation, metabolism, differentiation, senescence and apoptosis [25, 26]. Although MYC dysregulation is best known in cancer [27, 28]. c-Myc also participates in tissue remodeling and fibrosis in a context-dependent manner [29–31]. Recently, c-Myc has been found to be involved in the pathogenesis of fibrosis in multiple organs. For instance, c-Myc promotes renal fibrosis by inducing integrin αv-mediated TGF-β1 signaling [32]. In the liver, overexpression of c-Myc in hepatocytes promotes activation, proliferation and myofibroblast differentiation of hepatic stellate cells and facilitates the onset of liver fibrosis [33]. Moreover, pharmacological inhibition of MYC by 10058-F4 in the intestine improved high-fat, high-cholesterol and high-fructose diet (HFCFD)-induced liver fibrosis [34]. Conversely, endothelial c-Myc deletion exacerbates high-fat diet-induced liver inflammation and fibrosis [35]. However, despite these findings in other tissues, the specific role and underlying mechanisms of c-Myc in pulmonary fibrosis remain largely unexplored.

In the present study, we investigated whether c-Myc is altered in IPF and whether it functionally regulates profibrotic fibroblast behavior. We also explored whether and how c-Myc contributes to lung fibrosis through its pathogenic activity in lung fibroblasts. Gain- and loss-of-function experiments showed that c-Myc promoted fibroblast activation, proliferation, migration, ECM production and cellular senescence, at least in part through regulation of TGF-β1/Smad signaling. *In vivo*, we further demonstrated that adeno-associated virus serotype 9 (AAV9)-mediated c-Myc overexpression aggravated bleomycin (BLM)-induced pulmonary fibrosis and cellular senescence in mice. Finally, we showed that short hairpin RNA (shRNA)-mediated knockdown of c-Myc effectively alleviated the pro-fibrotic and senescent phenotypes in primary lung fibroblasts from patients with IPF. Collectively, our findings provide a proof-of-principle that c-Myc may serve as a viable therapeutic target against lung fibrosis.

2. Materials and Methods

2.1 Human lung tissue samples

Human lung tissue samples were collected from patients diagnosed with IPF (n = 22) and healthy donors (n = 26) at the First Affiliated Hospital of Guangzhou Medical University. For the healthy control group, morphologically and histologically normal lung tissues were obtained from the adjacent regions of surgically resected benign lung nodules. The diagnosis of IPF was established based on comprehensive physical examinations and chest high-resolution computed tomography (HRCT) findings, strictly adhering to the official American Thoracic Society (ATS)/European Respiratory Society (ERS) consensus diagnostic criteria [2]. Written informed consent was obtained from all participants prior to tissue collection. The study was approved by the Ethics Committee of the First Affiliated Hospital of

Guangzhou Medical University (Approval No.: 2021G-29). The baseline demographic and clinical characteristics of the study population are summarized in Table S1.

2.2 Single-cell RNA sequencing (scRNA-seq) and data analysis

Fresh human lung tissues from IPF patients and healthy donors were mechanically minced and digested with a mixture of Collagenase D (4 mg/mL) and DNase I (0.4 mg/mL) at 37°C for 45 min with gentle rotation. The digested cell suspensions were filtered through a 70-μm cell strainer, and red blood cells were removed using ACK lysis buffer. Cell viability was confirmed to be > 98%. The single-cell suspensions were then cryopreserved and subjected to scRNA-seq profiling performed by Beijing Biotech Co., Ltd. For data analysis, gene symbols were standardized according to the NCBI database.

2.3 Reagents and antibodies.

BLM was purchased from Hisun Pfizer Pharmaceuticals Co., Ltd. (Hangzhou, China), and recombinant TGF-β1 was purchased from Novoprotein (Shanghai, China). anti-c-Myc (ab32072, abcam), anti-FN (ab2413, abcam), anti-Col1 (ab260043, abcam; GB11022-3, Servicebio), anti-α-SMA (4904, Sigma-Aldrich; 19245, CST), anti-p53 (abs130506, absin), anti-p21 (abs149756, absin), anti-p16 (abs131586, absin), anti-Ki67 (abs130135, absin), anti-PCNA (AF0261, Beyotime Biotechnology), anti-p-Smad2 (18338, Cell Signaling), anti-Smad2 (5339, Cell Signaling), anti-p-Smad3 (9520, Cell Signaling), anti-Smad3 (9523, Cell Signaling), anti-GAPDH (5174, CST), and anti-Rabbit/Mouse IgG (H + L) (4904 and 4904, yeasen). All other reagents were purchased from GBCBIO Technologies Inc. (Guangzhou, China), unless otherwise stated.

2.4 Animal experimental protocols

C57BL/6 mice (8 weeks old) were obtained from Hunan SJA Laboratory Animal Co., Ltd (Changsha, Hunan, China), and were housed in a temperature-controlled specific pathogen-free barrier facility with a 12-hour light/dark cycle. All experimental protocols were approved by the Animal Care Committee of Guangzhou Medical University, China. Mice were anesthetized by 1.2% Avertin solution (20g/350μl) and received an intratracheal instillation of c-Myc-expressing AAV9 viral genome particles (AAV9-c-Myc OE, 2×10^{11} vg/mouse, PackGene Biotech, Guangzhou, China) or control AAV9-NC vectors. Fourteen days after AAV9 administration, BLM was administered intratracheally at a dose of 1.8 mg/kg body weight (or saline as controls) to induce pulmonary fibrosis. Mouse lungs were harvested on day 21 following the BLM challenge for subsequent analysis.

2.5 Micro-CT analysis.

Mice were anesthetized by isoflurane and transferred into an apparatus to scan the lungs. High-resolution scans (50 μm voxel size) were acquired using the Super Nova CT (PINGSENG Healthcare Inc., SNC-100, Kunshan, Jiangsu, China) according to the manufacturer's instructions and analyzed with the algorithms of three-dimensional (3D) finite element (AVATAR 1.5.0, PINGSENG Healthcare Inc., China).

2.6 Histopathology analysis.

Mouse left lungs were fixed in 4% neutral buffered formalin for 24 h, dehydrated, embedded in paraffin and sectioned at 5 μm. Histopathological analysis of paraffin-embedded lungs was performed in lung sections stained with hematoxylin and eosin (H&E) staining using standard procedures. Whereafter, the whole slide images (WSI) of pathology slides were scanned by the Aperio CS2 whole slides scanner (Leica, Germany). These digital images were converted to panoramic images by Aperio Image Scope (Version 12.3.2.5030, Leica Biosystems). Measurement of fibrotic area was quantified using an Orbit Image Analysis software (Actelion Pharmaceuticals Ltd, Allschwil, Switzerland) as previously reported.

2.7 Primary lung fibroblast cultures.

Primary lung fibroblasts were isolated from the human IPF lungs by combining trypsin digestion and tissue adherent methods, according to previously described methods. Briefly, the lung tissues from IPF patients were cut into small pieces and washed with phosphate-buffered saline (PBS) until the liquid was clear. Trypsin (2.5 mg/ml) was added to digest the tissue for 15 min. Lung tissue was moved into the culture flask, immersed in Dulbecco's modified Eagle's medium (DMEM, Gibco, USA) containing 10% fetal bovine serum (FBS), and placed flasks overnight in CO_2 incubator at 37°C. On the second day, the tissue blocks were washed with DMEM for 3 times, and the liquid was sucked away. The tissue block was placed evenly in the bottle. DMEM medium supplemented with 10% FBS was then added into the bottle, and the culture bottle was placed vertically in the cell incubator. After 3 hours, the bottle was gently laid down and maintained in the incubator.

2.8 Lentivirus packaging and transduction

Lentiviral vectors for c-Myc overexpression or shRNA-mediated knockdown were packaged in 293T cells. Briefly, 293T cells were cultured in 10-cm dishes until they reached approximately 80% confluence. The cells were then transfected with a mixture of the core transfer plasmid (6 μg), psPAX2 packaging plasmid (4 μg), and pMD2.G envelope plasmid (2 μg) using Lipofectamine 2000 (Thermo Fisher Scientific, USA) in serum-free DMEM. After 6 h of incubation, the transfection medium was replaced with fresh complete DMEM containing 10% FBS. Viral supernatants were collected at 24, 48, 72, and 96 h post-transfection and pooled together. The combined supernatant was centrifuged at 500 × *g* for 5 min at 4°C and filtered through a 0.22-μm filter to remove cell debris. The viral particles were then concentrated using a 100-kDa molecular weight cut-off (MWCO) centrifugal filter unit (Millipore, USA). The concentrated lentivirus was aliquoted and stored at -80°C. For viral transduction, primary lung fibroblasts were seeded in culture plates. When the cells reached 30–40% confluence, the concentrated lentivirus was added directly to the culture medium. The medium was replaced with fresh complete medium 24 h after transduction. Transduction efficiency was evaluated 48 h later by observing green fluorescent protein (GFP) expression under a fluorescence microscope (DM6B, Leica, Germany). The specific shRNA sequences targeting human c-Myc are listed in Table S2.

2.9 Immunofluorescence staining

Primary lung fibroblasts were seeded on glass slides in 12-well plates and incubated as indicated for 48 h. The slides were washed 3 times with PBS, fixed in 4% paraformaldehyde for 10 min, and then permeabilized with 0.1% Triton X-100 for 20 min. Cells were then blocked with 3% BSA at room temperature for 1 h followed by incubation with anti-Col1 (1:200 dilutions) at 4°C overnight. Slices were washed 3 times with PBS and incubated with a goat anti-mouse Cy3-conjugated IgG (1:300 dilution, Beyotime Institute of Biotechnology) for 1 h, and then labeled with DAPI for 5 min. Finally, slices were washed four times with PBS, mounted in antifade mounting medium, and visualized and photographed under a fluorescence microscope (DM6B, Leica, Germany).

2.10 EdU incorporation assay

Cell proliferation was evaluated using the BeyoClick™ EdU-555 Cell Proliferation Kit (Beyotime Biotechnology, China) according to the manufacturer's instructions. Briefly, primary IPF fibroblasts were seeded in 6-well plates and grown to approximately 80% confluence. Cells were incubated with 10 μM EdU working solution for 2 h at 37°C. Following incubation, cells were fixed with 4% paraformaldehyde for 15 min and permeabilized with 0.3% Triton X-100 for 10 min at room temperature. The cells were then incubated with the Click reaction cocktail for 30 min in the dark. Nuclei were subsequently counterstained with DAPI for 10 min. Images were captured using a fluorescence microscope, and the percentage of EdU-positive cells was quantified.

2.11 SA-β-Gal staining

SA-β-Gal staining was performed using PLFs grown on 12-well plates according to the manufacturer’s instructions (Beyotime Biotechnology, Jiangsu, China).

2.12 Wound healing assay.

Primary lung fibroblasts (transduced with c-Myc overexpression, c-Myc shRNA, or their respective control vectors) were seeded in 6-well plates. On attaining 100% confluence, a scratch was made using a sterile 200 μL micropipette tip. Then, the cells were washed with PBS, and the medium was changed to serum-free DMEM in the presence or absence of TGF-β1 (10 ng/mL) for 48 h. Images from six randomly selected fields along the scratched line in each well were obtained and analyzed by Image J software.

2.13 Transwell assay.

Primary lung fibroblasts (transduced with c-Myc overexpression, c-Myc shRNA, or their respective control vectors) were suspended in serum-free DMEM in the presence or absence of TGF-β1 (10 ng/mL) and seeded into the upper chamber of Transwell inserts (8 μm pore size). Meanwhile, 500 μl of DMEM containing 10% FBS was added to the lower chamber as a chemoattractant. After 48 h of incubation at 37°C, the cells remaining on the upper surface of the membrane were gently removed. The cells that migrated to the bottom surface were fixed with 4% paraformaldehyde and stained with 0.1% crystal violet for 10 min at room temperature. Images were obtained with a microscope (Leica, Germany) and counted using Image J software.

2.14 RNA extraction and reverse transcription quantitative real-time PCR (RT-qPCR)

Total RNA was extracted from tissues or cultured cells using QIAzol (Qiagen) and the miRNeasyMini Kit (Qiagen) in accordance with the manufacturer's protocol. For mRNA expression by RT-qPCR analysis, complementary DNA (cDNA) was prepared using a Color Reverse Transcription Kit (EZBioscience, USA), in which each reaction contained 1 μg of total RNA, according to the manufacturer's instructions. RT-qPCR was subsequently performed with cDNA using qPCR SYBR Green Master Mix (Yeasen, Shanghai, China). The data were collected and analysed using an iCyler iQ Real-time PCR Detection System (Bio-Rad Laboratories Inc., USA). All mRNA quantification data from cultured cells were normalized to the expression of 18s. All PCR primers were purchased from Thermo Fisher Scientific and are listed in Table S3.

2.15 Protein extraction and western blot analysis.

Proteins from lung tissues or primary lung fibroblasts were homogenized in RIPA lysis buffer with protease and phosphatase inhibitors (Roche) followed by centrifugation (4°C, 12000 rpm, 30 min) to clear the lysate. Lysate total protein concentration was measured using BCA Protein Assay Kit (Thermo Fisher Scientific, Waltham, MA, USA). Equal amounts (20 μg) of protein were loaded onto 10% SDS-polyacrylamide gels, transferred to polyvinylidene fluoride membranes (Millipore, MA, USA) and incubated with primary antibodies overnight at 4°C. After reacting with horseradish peroxidase (HRP)-labeled secondary antibodies (Yeasen, China), the immunoreactive bands were visualized using an ECL chemiluminescent kit (Yeason) and then scanned with Tanon-5200 (Tanon Science & Technology Co., Ltd., Shanghai, China).

2.16 Analysis of RNA-seq

Total RNA was extracted from primary IPF fibroblasts transduced with control (GFPTG) or c-Myc shRNA in the presence of TGF-β1. cDNA libraries were constructed using a KAPA RNA HyperPrep kit (Kapa Biosystems, Wilmington, MA, USA) following the manufacturer's protocol. The cDNA libraries were sequenced using an Illumina HiSeq X Ten system (Illumina, USA). The transcriptome data were analyzed by kallisto and Deseq2.

2.17 Statistical analysis

Data from at least three independent experiments are shown as the mean ± standard error of the mean (SEM). Statistical analyses were applied using Student's t-test and one-way analysis of variance to determine statistical significance. Analyses were performed with GraphPad Prism software (Version 6.07, USA). $P < 0.05$ was considered statistically significant in all experiments.

3. Results

3.1 c-Myc is substantially upregulated in the lung tissues and fibroblasts of IPF patients

To investigate the clinical relevance and potential pathogenic role of c-Myc in IPF, we first analyzed scRNA-seq datasets of lung tissues from healthy donors and IPF patients. Global clustering successfully identified distinct cellular populations within the lung microenvironment (Fig. 1A). Notably, dimensionality reduction plots revealed that c-Myc expression was selectively upregulated in IPF lungs (Fig. 1B). Further subpopulation analysis using violin plots confirmed that this upregulation was predominantly concentrated in fibroblasts in patients with IPF (Fig. 1C).

To substantiate these transcriptomic findings, we assessed the expression of c-Myc and classical ECM markers in clinical lung tissue cohorts. The basic demographic metadata of the healthy donors and IPF cohorts are presented in Table S1. RT-qPCR revealed a significant upregulation of c-Myc mRNA in IPF lungs relative to donor controls, which paralleled the increased transcription of fibrotic markers including Fibronectin, Collagen I, and α-SMA (Fig. 1D). Consistently, western blot analysis confirmed a striking accumulation of c-Myc protein in IPF tissues, accompanied by the excessive deposition of Fibronectin and Collagen I proteins (Fig. 1, E and F). To corroborate our tissue-level findings at the cellular level, we isolated and cultured primary lung fibroblasts from healthy donors and IPF patients. Consistent with the *in vivo* profiles, primary IPF fibroblasts exhibited an intrinsically activated basal phenotype, characterized by significantly elevated protein and mRNA levels of c-Myc, which was accompanied by the robust accumulation of Collagen I and Fibronectin (Fig. 1, G and H). Together, these data demonstrate that c-Myc is aberrantly overexpressed in IPF—particularly within the fibroblast population—both at the tissue level and in isolated primary cells, and its dysregulation strongly correlates with the profibrotic phenotype and ECM accumulation characteristic of the disease.

3.2 c-Myc promotes myofibroblast activation, proliferation, and migration in primary IPF fibroblasts

Given that TGF-β1 serves as the master regulator of myofibroblast differentiation, we first investigated its relationship with c-Myc expression. Stimulation of primary IPF fibroblasts with TGF-β1 (0–10 ng/mL) induced a marked, dose-dependent increase in c-Myc protein expression alongside the expected excessive ECM production (Fig. 2A), suggesting that c-Myc is actively recruited and upregulated by canonical profibrotic signaling. To directly evaluate the functional consequence of c-Myc upregulation, we established a gain-of-function model using a lentiviral c-Myc overexpression (c-Myc OE) system. Following the successful validation of the lentiviral vector in 293T cells, which exhibited high infection efficiency and robust induction of c-Myc and Flag at both mRNA and protein levels (Fig. S1, A and B), we transduced primary IPF fibroblasts (Fig. S1C). Strikingly, targeted overexpression of c-Myc alone was sufficient to profoundly upregulate the molecular markers of myofibroblast activation. Compared to control cells, c-Myc OE fibroblasts displayed a significant transcriptomic upregulation of myofibroblast activation and ECM markers, including Fibronectin, Collagen I, and α-SMA (Fig. 2B). These findings were

firmly supported at the translational level, where c-Myc OE drove a substantial accumulation of Fibronectin, Collagen I, and α-SMA proteins (Fig. 2, C and D).

Having established that c-Myc upregulates the molecular markers of myofibroblast activation, we next sought to determine whether this molecular shift translates into functional phenotypic alterations. Aberrant proliferation and enhanced motility are hallmark pathogenic behaviors of activated myofibroblasts during fibrogenesis. To assess the impact of c-Myc on cell growth, we performed an EdU incorporation assay. Fluorescence imaging revealed a significant increase in the number of actively synthesizing DNA (EdU-positive) cells following c-Myc OE compared to control cells (Fig. 2, E and F). This accelerated proliferative capacity was further corroborated by a marked upregulation of the cell proliferation marker Ki-67 at the protein level (Fig. 2G). In addition to hyperproliferation, we evaluated the migratory capacity of these fibroblasts. A wound-healing scratch assay demonstrated that c-Myc OE fibroblasts exhibited significantly faster wound closure rates, migrating more rapidly into the scratched area at 24 and 36 hours post-injury (Fig. 2, H and J). To rigorously validate this migratory advantage, we performed transwell migration assays across primary fibroblast lines derived from three independent IPF patients. Consistently, overexpression of c-Myc led to a significant increase in the number of migrating cells across all patient-derived lines (Fig. 2, I and K). Collectively, these *in vitro* results reveal that c-Myc functions as an active regulator that exacerbates the pathogenic behaviors of IPF fibroblasts by directly driving their activation, hyperproliferation, and migration.

3.3 c-Myc is upregulated in BLM-induced murine lungs, and its *in vivo* overexpression exacerbates pulmonary fibrosis

To determine the role of c-Myc *in vivo*, we first examined its expression in a BLM-induced mouse model of pulmonary fibrosis. Compared to control mice, BLM-treated mice showed a significant increase in c-Myc mRNA levels, which was consistent with the increased expression of the fibrotic markers Collagen I and Fibronectin (Fig. 3A). Western blot analysis also confirmed that the protein levels of c-Myc, Collagen I, and Fibronectin were substantially higher in the lung tissues of BLM-treated mice (Fig. 3B). These data indicate that c-Myc is upregulated during pulmonary fibrosis *in vivo*.

We next investigated whether c-Myc overexpression promotes lung fibrosis in animals. We packaged an AAV9 vector to overexpress c-Myc (AAV9-c-Myc OE) and confirmed its expression efficiency in mouse fibroblasts (Fig. 3C). Mice received an intratracheal instillation of the AAV9-c-Myc OE or a control vector (AAV9-NC) 14 days before BLM treatment, and lung tissues were collected 21 days after the BLM injury (Fig. 3D). We used Micro-CT imaging to evaluate the structural changes in the lungs. The 3D airway modeling and cross-sectional images (axial and coronal) showed that BLM treatment caused clear lung consolidation and structural distortion. Notably, mice pre-treated with AAV9-c-Myc OE showed more severe lung damage and a further decrease in total lung volume compared to the AAV9-NC + BLM group (Fig. 3, E and F). Consistently, histological examination of H&E-stained lung sections (Fig. 3H) confirmed that c-Myc overexpression significantly increased the percentage of the fibrotic area in the lungs

(Fig. 3G). Together, these *in vivo* results demonstrate that c-Myc promotes the progression of pulmonary fibrosis.

3.4 c-Myc knockdown abolishes TGF-β1-induced myofibroblast activation and ECM production

Having established that c-Myc overexpression exacerbates fibrogenesis, we next performed loss-of-function experiments to further substantiate its obligatory role in IPF fibroblast activation using a lentivirus-mediated shRNA silencing approach. We first evaluated three distinct shRNA sequences targeting human c-Myc in 293T cells (Fig. 4A). Among them, c-Myc shRNA 2 demonstrated the most robust knockdown efficiency at both the transcriptional and translational levels (Fig. 4, B and C), and was thus selected for all subsequent silencing experiments.

Next, we transduced primary IPF fibroblasts with the optimized c-Myc shRNA or a control lentivirus, followed by stimulation with or without TGF-β1. As expected, TGF-β1 stimulation potently induced the expression of myofibroblast activation and ECM markers, including Fibronectin, Collagen I, and α-SMA, in the control fibroblasts. Importantly, targeted depletion of c-Myc effectively blocked this profibrotic response. The c-Myc-silenced fibroblasts failed to upregulate the mRNA and protein levels of these fibrotic markers, even under robust TGF-β1 stimulation (Fig. 4, D and E). This significant blockade of myofibroblast transformation was further corroborated by immunofluorescence staining. While TGF-β1 treatment induced robust Collagen I production in the control cells, c-Myc knockdown significantly suppressed this Collagen I deposition, maintaining the fibroblasts in a quiescent-like state (Fig. 4, F and G). Together, these data firmly establish that c-Myc is an indispensable downstream effector required for TGF-β1-driven myofibroblast activation and ECM accumulation.

3.5 c-Myc is essential for TGF-β1-induced hyperproliferation and migration in IPF fibroblasts

Having demonstrated that c-Myc knockdown prevents myofibroblast differentiation and ECM production at the molecular level, we next evaluated its impact on the functional phenotypes of IPF fibroblasts. In control fibroblasts, TGF-β1 stimulation significantly increased the percentage of EdU-positive cells; however, this proliferative response was almost entirely abolished following c-Myc knockdown (Fig. 5, A and B). Consistently, while TGF-β1 treatment upregulated the expression of PCNA and Ki-67 in control cells, c-Myc-depleted fibroblasts remained in a low-proliferative state, failing to upregulate these markers even under TGF-β1 stimulation (Fig. 5C). We next investigated the impact of c-Myc deficiency on migratory capacity. In the wound-healing assay, control fibroblasts successfully closed the scratch area within 48 hours in response to TGF-β1, whereas c-Myc knockdown cells showed significantly delayed wound closure (Fig. 5, D and E). Consistently, transwell assays using primary fibroblasts from three different IPF patients showed similar reductions in cell migration. Across all patient-derived lines, the TGF-β1-induced enhancement in migration was significantly blocked following c-Myc knockdown (Fig. 5, F and G). Collectively, these findings indicate that c-Myc is indispensable for the TGF-β1-induced hyperproliferative and migratory programs in IPF fibroblasts.

3.6 c-Myc promotes cellular senescence and regulates TGF-β1/Smad signaling in IPF fibroblasts

Cellular senescence is a key feature of IPF that contributes to disease progression. We first assessed the expression of classic senescence markers. The mRNA levels of p53, p21, and p16 were significantly increased in primary IPF fibroblasts compared to healthy donor controls (Fig. 6A). Consistently, overexpression of c-Myc in IPF fibroblasts further increased the protein levels of these senescence markers (Fig. 6B). We confirmed this functional change using SA-β-gal staining across primary fibroblasts from three different IPF patients. The results showed that c-Myc overexpression significantly increased the percentage of senescent cells (Fig. 6C). We next evaluated whether c-Myc knockdown could inhibit this senescent phenotype. While TGF-β1 treatment increased the protein levels of p21 and p16 in control cells, c-Myc silencing effectively prevented this upregulation (Fig. 6D). Similarly, RT-qPCR analysis showed that the TGF-β1-induced increases in p53, p21, and Collagen I mRNA expression were significantly blocked following c-Myc knockdown (Fig. 6E). To explore the underlying molecular mechanisms, we examined the canonical TGF-β1/Smad signaling pathway. Western blot analysis revealed that c-Myc knockdown strongly reduced the phosphorylation of Smad2 and Smad3 induced by TGF-β1, indicating an impaired cellular response to profibrotic signaling (Fig. 6F).

To evaluate the broader impact of c-Myc depletion, we performed RNA sequencing (RNA-seq) on control and c-Myc shRNA fibroblasts treated with TGF-β1. Consistent with our functional assays, Gene Ontology (GO) and KEGG enrichment analyses revealed that c-Myc knockdown broadly suppressed profibrotic and pathogenic gene networks. Specifically, pathways related to ECM organization and ECM-receptor interactions were significantly downregulated, which directly supports our earlier observations of reduced collagen deposition (Fig. S2). Moreover, c-Myc depletion markedly inhibited networks associated with the cell cycle, cellular senescence, and the MAPK signaling cascade (Fig. 6, G and H). These transcriptomic profiles confirm that removing c-Myc systemically blunts the proliferative, senescent, and matrix-producing programs induced by TGF-β1. Together, these data demonstrate that c-Myc promotes cellular senescence and is required for the activation of the profibrotic TGF-β1/Smad signaling pathway in IPF fibroblasts.

4. Discussion

In this study, we identify c-Myc as a fibroblast-associated regulator of profibrotic activation and cellular senescence in IPF [36]. It is characterized by aberrant proliferation of activated myofibroblasts and pathological remodeling of the ECM, which causes the scarring and destruction of normal lung architecture and function [37]. Recent studies indicate that c-Myc is significantly activated after fibrogenic injury in multiple organs, implying that this protein might be implicated in the development of organ fibrosis [32–34]. Here, we provide evidence showing that: (i) c-Myc is substantially increased in the lungs of patients with IPF and is prominently located in IPF fibroblasts; (ii) c-Myc participates in TGF-β1-induced fibroblast activation, migration, and ECM production; (iii) c-Myc mediates the cellular

senescence of fibroblasts during IPF pathogenesis; and most importantly, (iv) AAV9-mediated c-Myc overexpression aggravates pulmonary fibrosis *in vivo*, while c-Myc downregulation can reduce the pro-fibrotic and senescent phenotypes in primary IPF fibroblasts. Together, these data support a model in which c-Myc amplifies fibroblast activation, senescence and matrix remodeling during pulmonary fibrosis.

Our findings extend previous observations that c-Myc participates in fibrogenesis in other organs [38]. Overexpression of c-Myc can induce cell cycle progression and cell proliferation [39]. Previous studies identified c-Myc+ fibroblasts in mouse obstructed kidneys, where c-Myc overexpression induced the differentiation of fibroblasts into myofibroblasts via the activation of TGF-β1 signaling [32], suggesting that c-Myc promotes pro-fibrotic responses. In the present study, we found that c-Myc levels were markedly increased in the lung fibroblasts of IPF patients and BLM-treated mice, driving collagen deposition and ultimately lung fibrosis, which is consistent with these previous observations. Although c-Myc has been reported to modulate phenotypic transitions in other cell types within pulmonary or vascular disorders—such as driving pulmonary arterial smooth muscle cell proliferation in pulmonary arterial hypertension (PAH) [40]—our current study selectively focused on its explicit role in lung fibroblasts during IPF progression.

While the pathogenic involvement of c-Myc in pulmonary fibrosis is increasingly recognized, its specific regulatory networks are only beginning to be elucidated. For example, a recent notable study demonstrated that c-Myc induces idiopathic pulmonary fibrosis via the modulation of the miR-9-5p-mediated TBPL1 axis, highlighting its crucial role in fibroblast proliferation and differentiation [41]. Other investigations have similarly linked the c-Myc signaling axis to aerobic glycolysis or epithelial-mesenchymal transition in fibrotic lungs [42, 43]. Despite these important advances, previous research has predominantly relied on murine models or immortalized human cell lines (e.g., HFL-1 and MRC-5) [41], which may not fully recapitulate the complex, disease-specific microenvironment of human IPF. Furthermore, these studies often restrict their mechanistic focus to specific non-coding RNAs or isolated downstream targets. Our study addresses these critical limitations by utilizing scRNA-seq to directly map c-Myc upregulation to human IPF fibroblast subpopulations and by employing patient-derived primary IPF fibroblasts for rigorous functional assays. Moving beyond specific miRNA pathways, our findings bridge a key mechanistic gap by showing that c-Myc simultaneously drives two core features of IPF: the hyperactivation of TGF-β1/Smad signaling and cellular senescence.

The TGF-β1/Smad2/3 signaling pathway plays a central role in fibroblast activation and differentiation, serving as a fundamental driver in the development of pulmonary fibrosis [44]. For instance, enhanced p-Smad2/3 levels have been consistently observed in the lung fibroblasts of IPF patients, implying that elevated TGF-β activity dictates the fibrotic progression of IPF [8]. In the present study, we demonstrated that c-Myc knockdown effectively suppressed the hyperactivation of the canonical TGF-β1/Smad2/3 signaling pathway. Consequently, the blockade of this signaling cascade significantly attenuated TGF-β1-induced myofibroblast differentiation, migration, and excessive ECM production. These findings suggest

that c-Myc is not only induced by TGF-β1 but may also help maintain or amplify cellular responsiveness to TGF-β1/Smad signaling.

Cellular senescence, a state of permanent cell cycle arrest, contributes significantly to the age-related decline in tissue regenerative capacity and the pathophysiology of aging-related diseases, including IPF [45, 46]. Multiple cell types, including alveolar epithelial cells, endothelial cells, macrophages, and fibroblasts, have been shown to undergo senescence in IPF lungs [47]. Crucially, cellular senescence in fibroblasts directly facilitates myofibroblast differentiation and persistent fibrogenesis [22]. In our *in vitro* models, TGF-β1 stimulation robustly induced cellular senescence in primary IPF lung fibroblasts, consistent with previous reports [18, 48]. c-Myc overexpression enhanced these senescent phenotypes, whereas c-Myc knockdown attenuated SA-β-gal activity and reduced senescence-marker expression. Furthermore, senescent cells characteristically develop a SASP, releasing a myriad of pro-inflammatory cytokines and chemokines [49]. Although we observed changes in senescence markers and SA-β-gal activity, the full SASP program and its functional contribution were not comprehensively tested. Interestingly, the pro-senescent role of c-Myc in IPF fibroblasts parallels the well-documented phenomenon of oncogene-induced senescence (OIS) observed in various malignancies, such as osteosarcoma and lymphoma, where aberrant c-Myc hyperactivation triggers a senescent response [31]. *In vivo*, our data further corroborated this axis, revealing that AAV9-mediated c-Myc overexpression markedly exacerbated cellular senescence and senescence-associated marker expression in the lungs of BLM-injured mice. Given that canonical Smad2/3 signaling is a critical driver of cellular senescence in IPF [50], the anti-senescent effects achieved via c-Myc knockdown can likely be attributed to the concurrent uncoupling of the TGF-β1/Smad2/3 cascade.

In summary, our study demonstrated that c-Myc is significantly upregulated in the lungs and primary fibroblasts of IPF patients, as well as in BLM-injured mice. Mechanistically, targeted c-Myc inhibition effectively suppressed the activation and differentiation of IPF fibroblasts into myofibroblasts while mitigating cellular senescence *in vitro*, whereas AAV9-mediated c-Myc overexpression exacerbated these fibrotic and senescent phenotypes *in vivo*. However, we acknowledge certain limitations in the present study. Notably, while our data definitively establish c-Myc as a critical disease driver, we have not yet evaluated the efficacy of targeted *in vivo* therapeutic interventions, such as the post-injury administration of pharmacological c-Myc inhibitors or fibroblast-specific conditional knockout in animal models. Addressing these therapeutic windows and evaluating the safety profile of systemic c-Myc inhibition will be the primary focus of our future investigations to bridge the bench-to-bedside gap. Nonetheless, our findings provide compelling proof-of-concept that targeting the c-Myc signaling axis represents a promising translational strategy for the treatment of pulmonary fibrosis in clinical settings.

5. Conclusions

c-Myc is substantially upregulated in idiopathic pulmonary fibrosis and functions as a critical driver that promotes myofibroblast activation, extracellular matrix production, and cellular senescence via the canonical TGF-β1/Smad signaling pathway. While *in vivo* c-Myc overexpression exacerbates bleomycin-

induced lung injury, targeted knockdown of c-Myc effectively uncouples these profibrotic responses and mitigates the senescent phenotype. These findings highlight c-Myc as an indispensable amplifier of the fibrogenic network and identify it as a promising therapeutic target for preventing or attenuating pulmonary fibrosis.

Abbreviations

3D
Three-dimensional
AAV9
Adeno-associated virus serotype 9
ATS
American Thoracic Society
BLM
Bleomycin
c-Myc OE
c-Myc overexpression
cDNA
Complementary DNA
Con
Control
DMEM
Dulbecco’s modified Eagle’s medium
ECM
Extracellular matrix
ERS
European Respiratory Society
FBS
Fetal bovine serum
GFP
Green fluorescent protein
GO
Gene Ontology
H&E
Hematoxylin and eosin
HFCFD
High-fat, high-cholesterol and high-fructose diet
HRCT
High-resolution computed tomography
HRP

Horseradish peroxidase

ILDs

Interstitial lun

IPF

Idiopathic pulmonary fibrosis

MWCO

Molecular weight cut-off

NSIP

Non-specific interstitial pneumonia

OIS

Oncogene-induced senescence

PAH

Pulmonary arterial hypertension

PBS

Phosphate-buffered saline

ROS

Reactive oxygen species

RT-qPCR

Reverse transcription quantitative real-time PCR

SA-β-gal

Senescence-associated β-galactosidase

SASP

Senescence-associated secretory phenotype

scRNA-seq

Single-cell RNA sequencing

SEM

Standard error of the mean

shRNA

Short hairpin RNA

TGF-β1

Transforming growth factor-β1

TβRI

TGF-β receptor type I

TβRII

TGF-β receptor type II

WSI

Whole slide images

α-SMA

α-smooth muscle actin

Declarations

Ethics approval and consent to participate: This study was approved by the Ethics Committee of the First Affiliated Hospital of Guangzhou Medical University (Approval No.: 2021G-29). Written informed consent was obtained from all participants prior to tissue collection. All animal experimental protocols were reviewed and approved by the Animal Care Committee of Guangzhou Medical University, China.

Consent for publication: Not applicable.

Availability of data and materials: The datasets used and/or analysed during the current study are available from the corresponding author on reasonable request.

Competing interests: The authors declare that they have no competing interests.

Funding: This work was supported by the National Natural Science Foundation of China (82470061), Guangdong basic and applied basic research foundation (2025A1515010159), Guangzhou science and technology plan project (2025A03J4309).

Authors' contributions: PY and XC are the guarantors of the article and take responsibility for the integrity of the work as a whole, from inception to published article. PY and XC conceived the idea for this manuscript, designed the experiments. XP and YM contributed equally to this work, performed the majority of the *in vitro* and *in vivo* experiments, and took the lead in data analysis and interpretation. RG, HY, YW, HL, and JY were all directly involved in the execution of the study, assisted in the acquisition of data, and provided technical support for the molecular assays and animal models. All authors read and approved the final manuscript.

Acknowledgments: The authors thank the patients involved in this study and the clinical staff at the First Affiliated Hospital of Guangzhou Medical University for providing the clinical tissue samples and medical records.

References

1. Richeldi L, Collard HR, Jones MG. Idiopathic pulmonary fibrosis. Lancet. 2017;389:1941–52.
2. Raghu G, Remy-Jardin M, Richeldi L, Thomson CC, Inoue Y, Johkoh T, Kreuter M, Lynch DA, Maher TM, Martinez FJ, et al. Idiopathic Pulmonary Fibrosis (an Update) and Progressive Pulmonary Fibrosis in Adults: An Official ATS/ERS/JRS/ALAT Clinical Practice Guideline. Am J Respir Crit Care Med. 2022;205:e18–47.
3. Spagnolo P, Guler SA, Chaudhuri N, Udwadia Z, Sesé L, Kaul B, Enghelmayer JI, Valenzuela C, Malhotra A, Ryerson CJ, et al. Global epidemiology and burden of interstitial lung disease. Lancet Respir Med. 2025;13:739–55.
4. Spagnolo P, Kropski JA, Jones MG, Lee JS, Rossi G, Karampitsakos T, Maher TM, Tzouvelekis A, Ryerson CJ. Idiopathic pulmonary fibrosis: Disease mechanisms and drug development. Pharmacol

Ther. 2021;222:107798.
5. Maher TM. Interstitial Lung Disease: A Review. JAMA. 2024;331:1655–65.
6. Liu GY, Budinger GRS, Dematte JE. Advances in the management of idiopathic pulmonary fibrosis and progressive pulmonary fibrosis. BMJ. 2022;377:e066354.
7. Richeldi L, Azuma A, Cottin V, Kreuter M, Maher TM, Martinez FJ, Oldham JM, Valenzuela C, Clerisme-Beaty E, Gordat M, et al. Nerandomilast in Patients with Idiopathic Pulmonary Fibrosis. N Engl J Med. 2025;392:2193–202.
8. Wang Q, Xie ZL, Wu Q, Jin ZX, Yang C, Feng J. Role of various imbalances centered on alveolar epithelial cell/fibroblast apoptosis imbalance in the pathogenesis of idiopathic pulmonary fibrosis. Chin Med J (Engl). 2021;134:261–74.
9. Ziehr DR, Li F, Parnell KM, Krah NM, Leahy KJ, Guillermier C, Gao C, Prell SA, Vigder N, Poli S, et al. Lactate transport inhibition therapeutically reprograms fibroblast metabolism in experimental pulmonary fibrosis. Sci Transl Med. 2026;18:eads2673.
10. Watanabe N, Yoshida M, Hirano Y, Fujimoto S, Matsubayashi S, Ishiguro T, Takahashi N, Shimizu Y, Takayanagi N, Kawabata Y et al. Integrated spatial and single-cell transcriptomics reveal PAK kinase as a therapeutic target in fibroblastic foci and dense fibrosis of idiopathic pulmonary fibrosis. Eur Respir J 2025, 66.
11. Zhao H, Bian H, Bu X, Zhang S, Zhang P, Yu J, Lai X, Li D, Zhu C, Yao L, Su J. Targeting of Discoidin Domain Receptor 2 (DDR2) Prevents Myofibroblast Activation and Neovessel Formation During Pulmonary Fibrosis. Mol Ther. 2016;24:1734–44.
12. Misharin AV, Budinger GRS. Targeting the Myofibroblast in Pulmonary Fibrosis. Am J Respir Crit Care Med. 2018;198:834–5.
13. Fang YF, Zhang C, Han MM, Wang Y, Zhou TJ, Xing L, Wei N, Wang J, Jeong JH, Zhou F, et al. Engineered MSCs Break Endothelial-Myofibroblast Crosstalk in Pulmonary Fibrosis: Reconstructing the Vascular Niche. Adv Mater. 2025;37:e2414601.
14. Kim S, Kim Y, Kim TS, Kang JH, Yun IY, Lee ES, Lee EJ, Kim RK, Yi JM, Choi HS, et al. Colony-stimulating factor 3 as a key mediator in the progression of idiopathic pulmonary fibrosis: a novel therapeutic target. Signal Transduct Target Ther. 2025;10:322.
15. Moss BJ, Ryter SW, Rosas IO. Pathogenic Mechanisms Underlying Idiopathic Pulmonary Fibrosis. Annu Rev Pathol. 2022;17:515–46.
16. Maus M, López-Polo V, Mateo L, Lafarga M, Aguilera M, De Lama E, Meyer K, Sola A, Lopez-Martinez C, López-Alonso I, et al. Iron accumulation drives fibrosis, senescence and the senescence-associated secretory phenotype. Nat Metab. 2023;5:2111–30.
17. Liu RM, Liu G. Cell senescence and fibrotic lung diseases. Exp Gerontol. 2020;132:110836.
18. Álvarez D, Cárdenes N, Sellarés J, Bueno M, Corey C, Hanumanthu VS, Peng Y, D'Cunha H, Sembrat J, Nouraie M, et al. IPF lung fibroblasts have a senescent phenotype. Am J Physiol Lung Cell Mol Physiol. 2017;313:L1164–73.

19. Hecker L, Logsdon NJ, Kurundkar D, Kurundkar A, Bernard K, Hock T, Meldrum E, Sanders YY, Thannickal VJ. Reversal of persistent fibrosis in aging by targeting Nox4-Nrf2 redox imbalance. Sci Transl Med. 2014;6:231ra247.
20. Schuliga M, Read J, Blokland KEC, Waters DW, Burgess J, Prêle C, Mutsaers SE, Jaffar J, Westall G, Reid A, et al. Self DNA perpetuates IPF lung fibroblast senescence in a cGAS-dependent manner. Clin Sci (Lond). 2020;134:889–905.
21. Okuda R, Aoshiba K, Matsushima H, Ogura T, Okudela K, Ohashi K. Cellular senescence and senescence-associated secretory phenotype: comparison of idiopathic pulmonary fibrosis, connective tissue disease-associated interstitial lung disease, and chronic obstructive pulmonary disease. J Thorac Dis. 2019;11:857–64.
22. Guan R, Yuan L, Li J, Wang J, Li Z, Cai Z, Guo H, Fang Y, Lin R, Liu W et al. Bone morphogenetic protein 4 inhibits pulmonary fibrosis by modulating cellular senescence and mitophagy in lung fibroblasts. Eur Respir J 2022, 60.
23. Lu Q, Ye C, Mao W, Zeng F, Liu Z, Chen R, Cheng X, Gao Y, Wang M, Liu M, et al. Targeting Senescent Alveolar Type 2 Cells with a Gene-Editable FePt Dual-Atom Catalyst for Mitigating Idiopathic Pulmonary Fibrosis. ACS Nano. 2025;19:23162–76.
24. Barnes PJ, Baker J, Donnelly LE. Cellular Senescence as a Mechanism and Target in Chronic Lung Diseases. Am J Respir Crit Care Med. 2019;200:556–64.
25. van Riggelen J, Yetil A, Felsher DW. MYC as a regulator of ribosome biogenesis and protein synthesis. Nat Rev Cancer. 2010;10:301–9.
26. Wang C, Zhang J, Yin J, Gan Y, Xu S, Gu Y, Huang W. Alternative approaches to target Myc for cancer treatment. Signal Transduct Target Ther. 2021;6:117.
27. Hofmann JW, Zhao X, De Cecco M, Peterson AL, Pagliaroli L, Manivannan J, Hubbard GB, Ikeno Y, Zhang Y, Feng B, et al. Reduced expression of MYC increases longevity and enhances healthspan. Cell. 2015;160:477–88.
28. Dang CV. MYC on the path to cancer. Cell. 2012;149:22–35.
29. Tan JP, Liu X, Polo JM. Establishment of human induced trophoblast stem cells via reprogramming of fibroblasts. Nat Protoc. 2022;17:2739–59.
30. Chappell J, Dalton S. Roles for MYC in the establishment and maintenance of pluripotency. Cold Spring Harb Perspect Med. 2013;3:a014381.
31. Takahashi K, Yamanaka S. Induction of pluripotent stem cells from mouse embryonic and adult fibroblast cultures by defined factors. Cell. 2006;126:663–76.
32. Shen Y, Miao N, Wang B, Xu J, Gan X, Xu D, Zhou L, Xue H, Zhang W, Yang L, Lu L. c-Myc promotes renal fibrosis by inducing integrin αv-mediated transforming growth factor-β signaling. Kidney Int. 2017;92:888–99.
33. Nevzorova YA, Cubero FJ, Hu W, Hao F, Haas U, Ramadori P, Gassler N, Hoss M, Strnad P, Zimmermann HW, et al. Enhanced expression of c-myc in hepatocytes promotes initiation and progression of alcoholic liver disease. J Hepatol. 2016;64:628–40.

34. Luo Y, Yang S, Wu X, Takahashi S, Sun L, Cai J, Krausz KW, Guo X, Dias HB, Gavrilova O, et al. Intestinal MYC modulates obesity-related metabolic dysfunction. Nat Metab. 2021;3:923–39.
35. Qi Y, Qadir MMF, Hastreiter AA, Fock RA, Machi JF, Morales AA, Wang Y, Meng Z, Rodrigues CO. Endothelial c-Myc knockout enhances diet-induced liver inflammation and fibrosis. Faseb j. 2022;36:e22077.
36. Bonella F, Spagnolo P, Ryerson C. Current and Future Treatment Landscape for Idiopathic Pulmonary Fibrosis. Drugs. 2023;83:1581–93.
37. Wang J, Lai X, Yao S, Chen H, Cai J, Luo Y, Wang Y, Qiu Y, Huang Y, Wei X et al. Nestin promotes pulmonary fibrosis via facilitating recycling of TGF-β receptor I. Eur Respir J 2022, 59.
38. Levens D. Cellular MYCro economics: Balancing MYC function with MYC expression. Cold Spring Harb Perspect Med 2013, 3.
39. Zlotorynski E. MYC in TOP shape. Nat Rev Mol Cell Biol. 2022;23:92.
40. Zhang C, Ma C, Zhang L, Zhang L, Zhang F, Ma M, Zheng X, Mao M, Shen T, Zhu D. MiR-449a-5p mediates mitochondrial dysfunction and phenotypic transition by targeting Myc in pulmonary arterial smooth muscle cells. J Mol Med (Berl). 2019;97:409–22.
41. Qin H, Tang Y, Mao Y, Zhou X, Xu T, Liu W, Su X. C-MYC induces idiopathic pulmonary fibrosis via modulation of miR-9-5p-mediated TBPL1. Cell Signal. 2022;93:110274.
42. Zhang J, Chen W, Du J, Chu L, Zhou Z, Zhong W, Liu D, Huang H, Huang Y, Qiao Y, et al. RNF130 protects against pulmonary fibrosis through suppressing aerobic glycolysis by mediating c-myc ubiquitination. Int Immunopharmacol. 2023;117:109985.
43. Yang J, Jiang G, Ni K, Fan L, Tong W, Yang J. Emodin inhibiting epithelial-mesenchymal transition in pulmonary fibrosis through the c-MYC/miR-182-5p/ZEB2 axis. Phytother Res. 2023;37:926–34.
44. Guan R, Zhao X, Wang X, Song N, Guo Y, Yan X, Jiang L, Cheng W, Shen L. Emodin alleviates bleomycin-induced pulmonary fibrosis in rats. Toxicol Lett. 2016;262:161–72.
45. Calcinotto A, Kohli J, Zagato E, Pellegrini L, Demaria M, Alimonti A. Cellular Senescence: Aging, Cancer, and Injury. Physiol Rev. 2019;99:1047–78.
46. Childs BG, Durik M, Baker DJ, van Deursen JM. Cellular senescence in aging and age-related disease: from mechanisms to therapy. Nat Med. 2015;21:1424–35.
47. Roque W, Romero F. Cellular metabolomics of pulmonary fibrosis, from amino acids to lipids. Am J Physiol Cell Physiol. 2021;320:C689–95.
48. Schuliga M, Pechkovsky DV, Read J, Waters DW, Blokland KEC, Reid AT, Hogaboam CM, Khalil N, Burgess JK, Prêle CM, et al. Mitochondrial dysfunction contributes to the senescent phenotype of IPF lung fibroblasts. J Cell Mol Med. 2018;22:5847–61.
49. Gorgoulis V, Adams PD, Alimonti A, Bennett DC, Bischof O, Bishop C, Campisi J, Collado M, Evangelou K, Ferbeyre G, et al. Cellular Senescence: Defining a Path Forward. Cell. 2019;179:813–27.

50. Milara J, Ballester B, Montero P, Escriva J, Artigues E, Alós M, Pastor-Clerigues A, Morcillo E, Cortijo J. MUC1 intracellular bioactivation mediates lung fibrosis. Thorax. 2020;75:132–42.

Figures

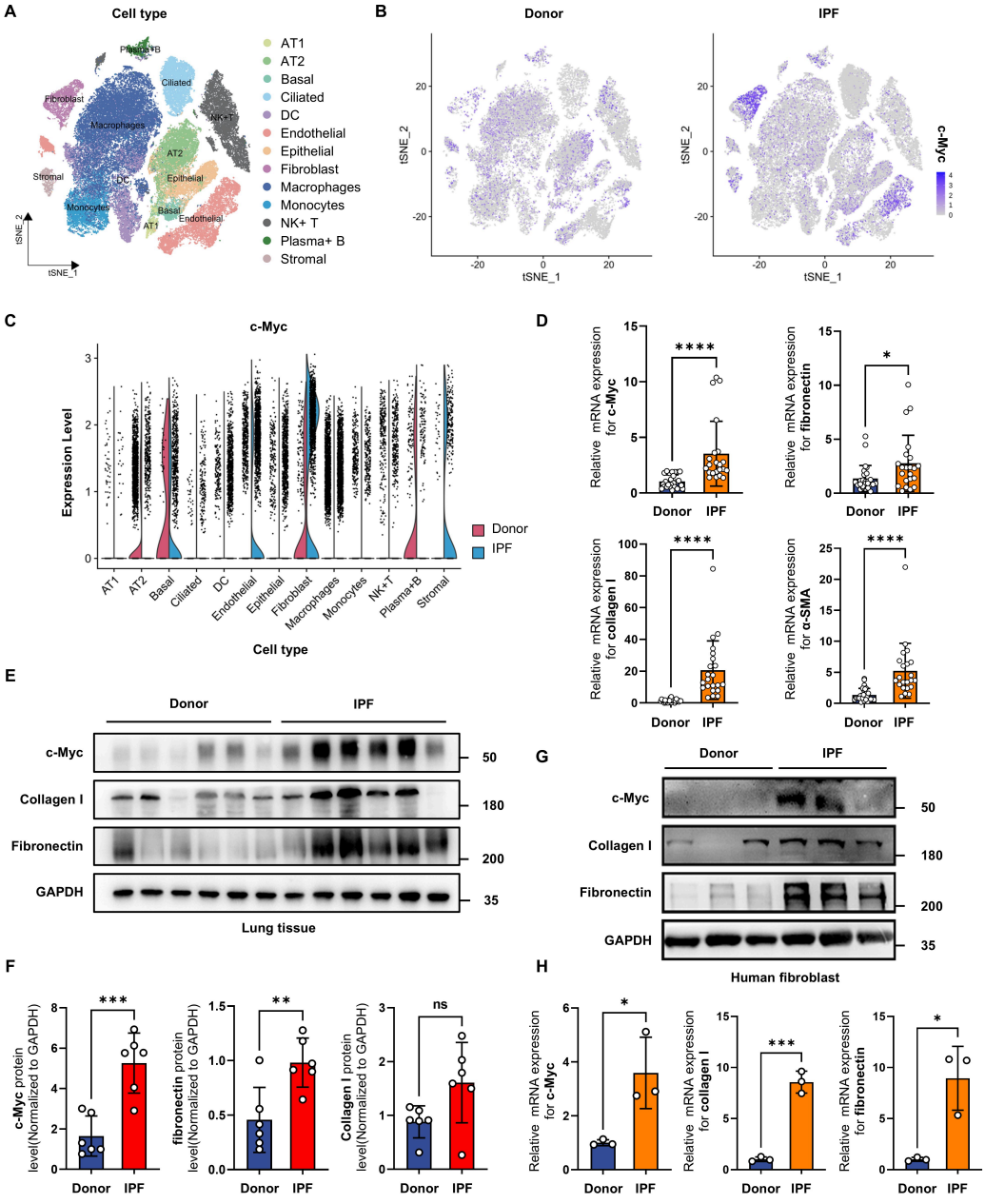


Figure 1

Expression patterns of c-Myc and fibrotic markers in clinical IPF cohorts and patient-derived primary fibroblasts. (A) Cell type annotation and clustering of scRNA-seq data from human lung tissues visualized by t-SNE plot. **(B)** t-SNE feature plots comparing c-Myc expression patterns in healthy donors (left) versus IPF patients (right). **(C)**Violin plots illustrating the expression levels of c-Myc across diverse cell types in donor (red) versus IPF (blue) lung tissues. **(D)** RT-qPCR analysis of c-Myc, Fibronectin, Collagen I, and α-SMA mRNA expression in lung tissues from healthy donors and IPF patients. **(E)** Representative western blot images of c-Myc, Collagen I, and Fibronectin protein levels in lung tissue homogenates from donors and IPF patients. GAPDH was used as the loading control. **(F)** Densitometric quantification of c-Myc, Fibronectin, and Collagen I protein levels normalized to GAPDH. **(G)** Representative western blot images of c-Myc, Collagen I, and Fibronectin protein expression in primary lung fibroblasts isolated from healthy donors and IPF patients. **(H)**RT-qPCR analysis of c-Myc, Collagen I, and Fibronectin mRNA expression in primary lung fibroblasts isolated from healthy donors and IPF patients. Data are presented as mean ± SEM. Statistical significance was determined using Student's t-test (*$p < 0.05$, $p < 0.01$, ***$p < 0.001$, ****$p < 0.0001$, ns = not significant).

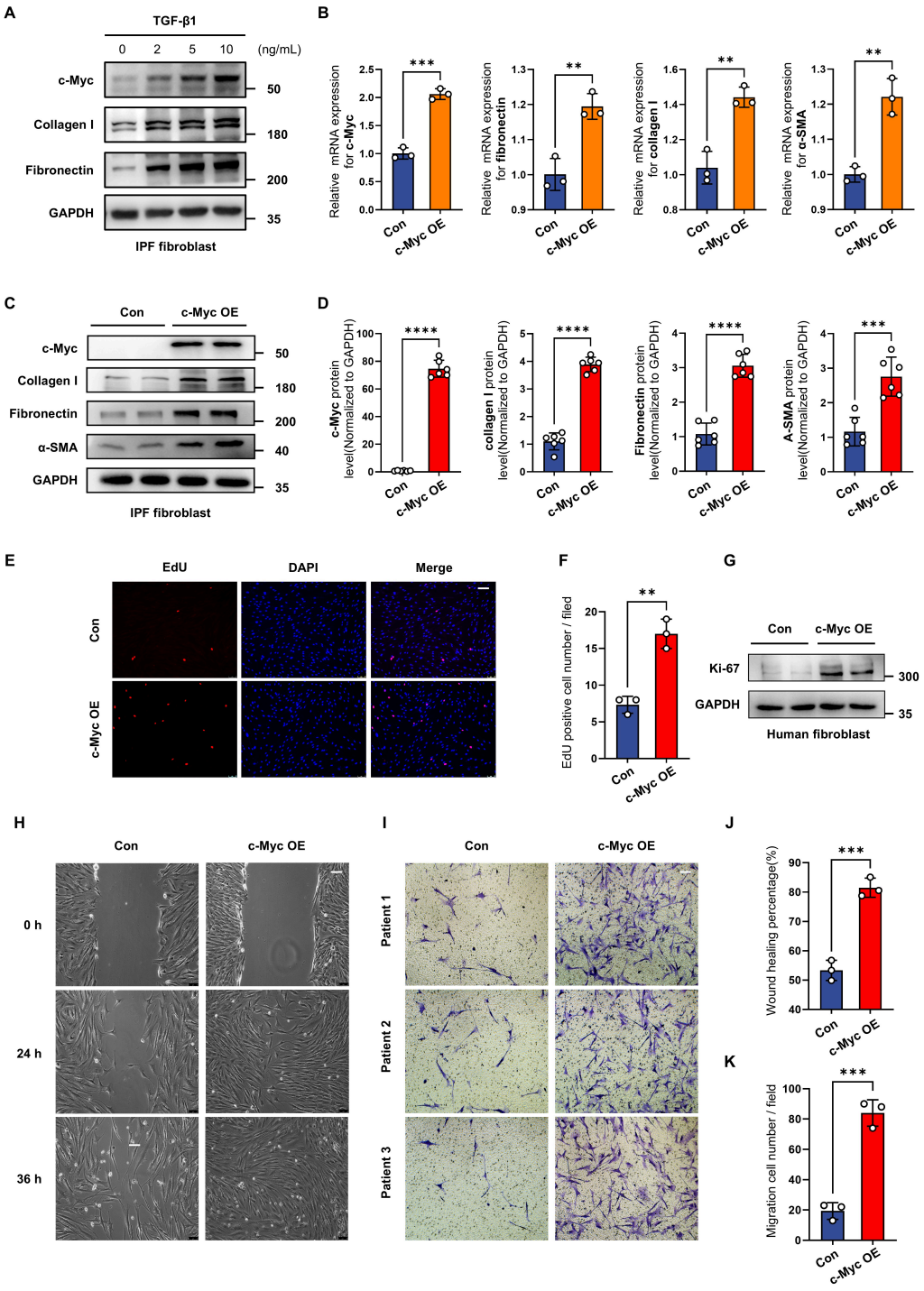


Figure 2

Functional impact of c-Myc overexpression on the activation, proliferation, and migratory capacities of primary IPF fibroblasts. (A) Western blot analysis of c-Myc, Collagen I, and Fibronectin protein expression in primary IPF fibroblasts treated with the indicated concentrations of TGF-β1 (0, 2, 5, and 10 ng/mL) for 48 h. **(B)** RT-qPCR analysis of c-Myc, Fibronectin, Collagen I, and α-SMA mRNA levels in primary IPF fibroblasts following transduction with control (Con) or lentiviral c-Myc overexpression (c-

Myc OE) vectors. **(C and D)** Representative western blot images **(C)**and corresponding densitometric quantification **(D)** of c-Myc, Collagen I, Fibronectin, and α-SMA protein expression in Con and c-Myc OE IPF fibroblasts. GAPDH was used as the loading control. **(E and F)** Representative fluorescence images of the EdU incorporation assay **(E)** and quantitative analysis of EdU-positive cells per field **(F)** in Con and c-Myc OE IPF fibroblasts. **(G)** Western blot analysis of the proliferation marker Ki-67 in Con and c-Myc OE IPF fibroblasts. **(H and J)** Representative brightfield images of the wound-healing assay captured at 0, 24, and 36 hours post-scratch **(H)**, alongside the quantification of the wound healing percentage **(J)**. **(I and K)** Representative images of the transwell migration assay utilizing primary fibroblasts derived from three independent IPF patients (Patient 1, Patient 2, and Patient 3) **(I)**, and the corresponding quantification of migrating cells per field **(K)**. Data are presented as mean ± SEM. Statistical significance was determined using Student's t-test (*$p < 0.05$, **$p < 0.01$, ***$p < 0.001$, ****$p < 0.0001$).

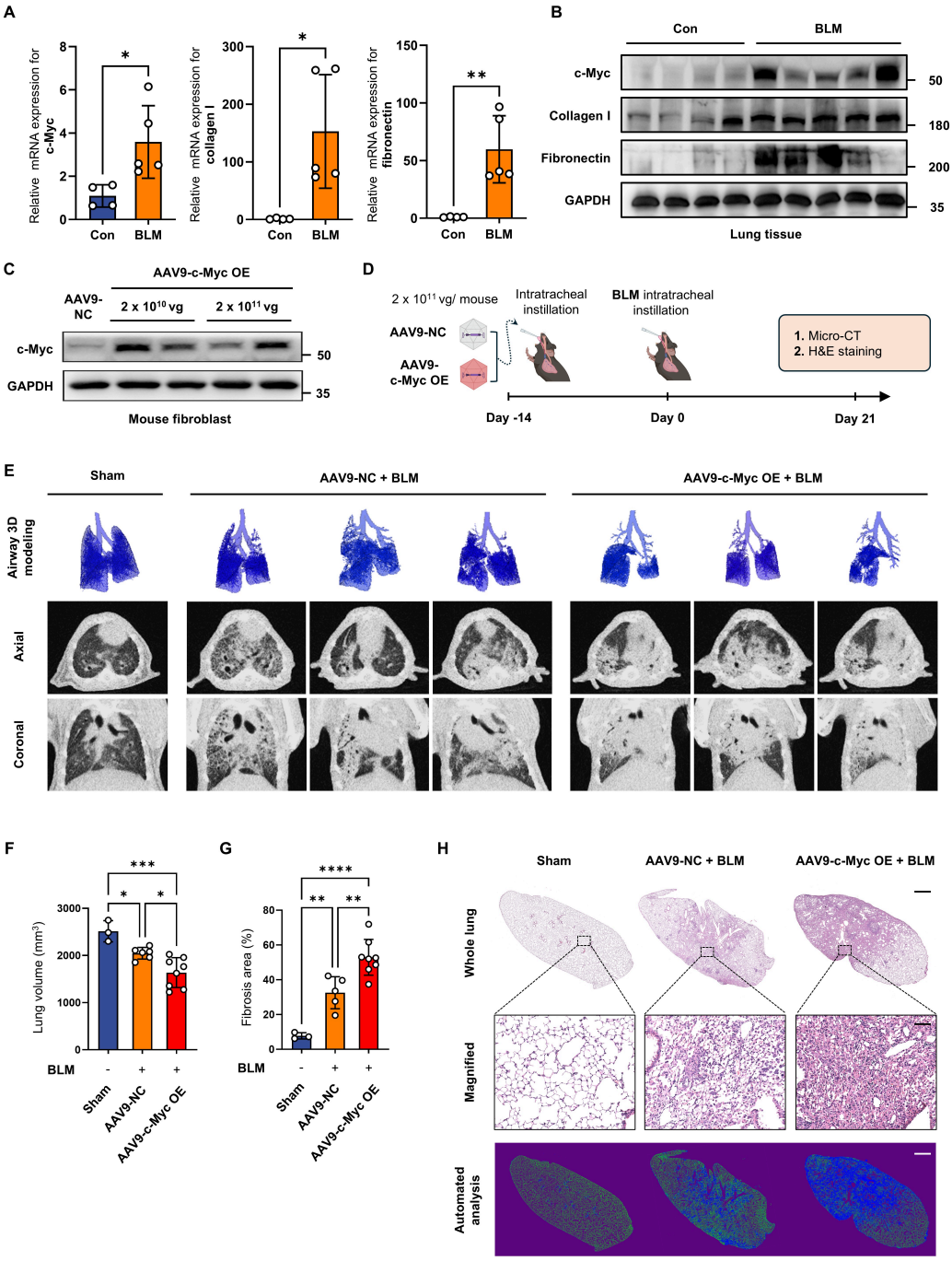


Figure 3

Expression of c-Myc in BLM-treated mice and the effect of its overexpression on pulmonary fibrosis. **(A)**RT-qPCR analysis of c-Myc, Collagen I, and Fibronectin mRNA expression in the lung tissues of control (Con) and BLM-treated mice. **(B)** Western blot analysis of c-Myc, Collagen I, and Fibronectin protein levels in the indicated mouse lung tissues. GAPDH served as the loading control. **(C)** Western blot validation of c-Myc overexpression in mouse fibroblasts transduced with different doses of AAV9-c-Myc

OE or a control vector (AAV9-NC). **(D)**Schematic diagram of the animal experimental design. Mice received an intratracheal instillation of AAV9 vectors 14 days prior to BLM injury, and lung tissues were evaluated at day 21 post-BLM. **(E)** Representative Micro-CT images, including airway 3D modeling, axial, and coronal views, of mouse lungs from the Sham, AAV9-NC+BLM, and AAV9-c-Myc OE+BLM groups. **(F)**Quantitative analysis of the total lung volume in the indicated groups. **(G)**Quantitative analysis of the percentage of fibrosis area in the indicated groups. **(H)** Representative H&E staining of whole lung sections (top row; scale bar: 1000 μm) and magnified views (middle row; scale bar: 50 μm), alongside the corresponding automated histological analysis images (bottom row; scale bar: 1000 μm) evaluating the damaged areas (green: normal lung tissue; blue: fibrotic lesions). Data are presented as mean ± SEM. Statistical significance was determined using Student's t-test (*$p < 0.05$, **$p < 0.01$, ***$p < 0.001$, ****$p < 0.0001$, ns = not significant).

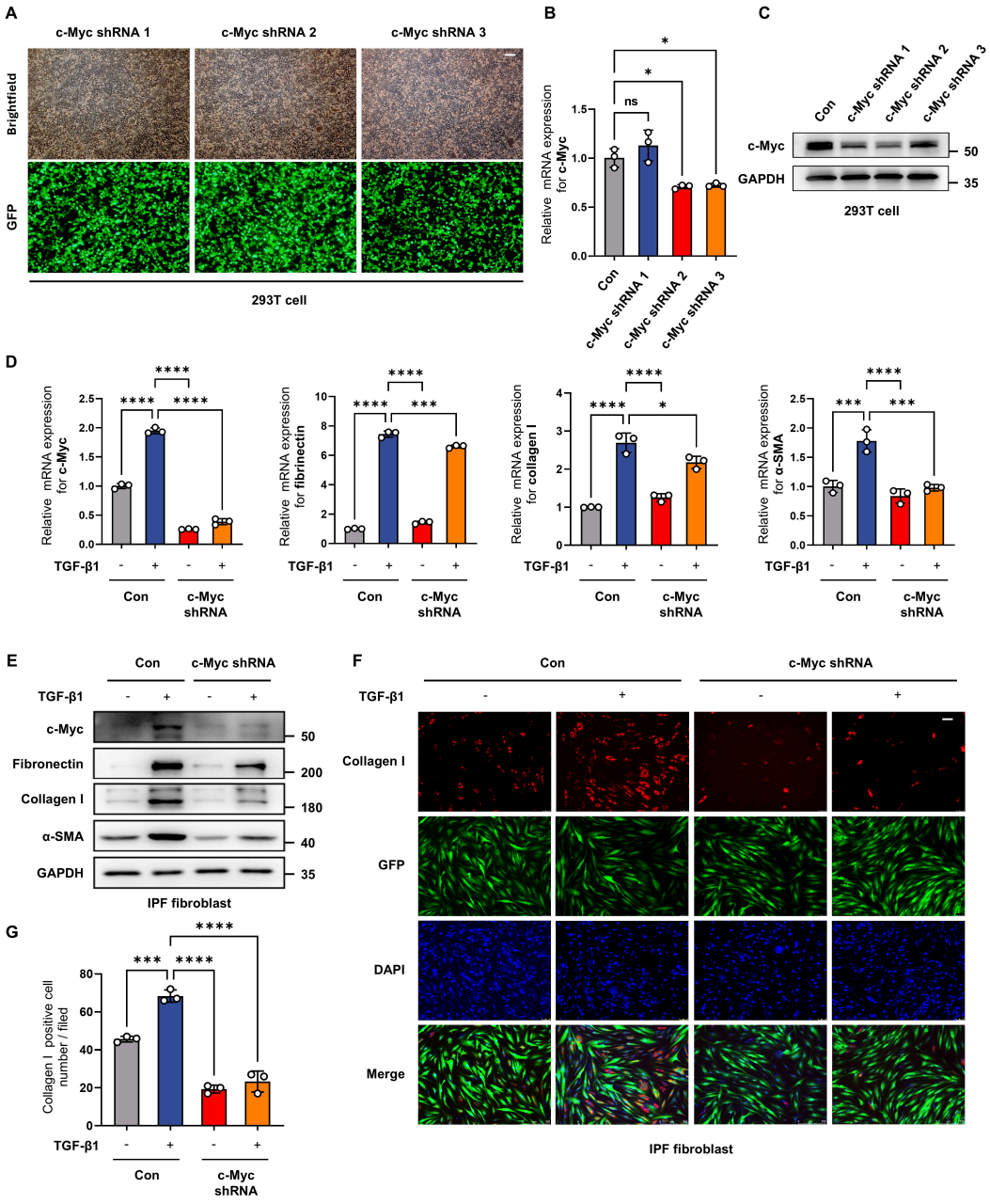


Figure 4

Impact of targeted c-Myc knockdown on TGF-β1-induced myofibroblast activation and ECM production in primary IPF fibroblasts. (A) Representative brightfield and fluorescence images demonstrating the transduction efficiency of three different lentiviral c-Myc shRNA constructs (shRNA 1, 2, and 3) in 293T cells. Scale bar: 250 μm. **(B and C)** RT-qPCR (B) and western blot analysis (C) evaluating the knockdown efficiency of the three c-Myc shRNA sequences in 293T cells. GAPDH served as the loading control. **(D)**

RT-qPCR analysis of c-Myc, Fibronectin, Collagen I, and α-SMA mRNA expression in primary IPF fibroblasts transduced with control (Con) or c-Myc shRNA, followed by treatment with or without TGF-β1 (10 ng/mL) for 48 h. **(E)**Representative western blot images showing the protein levels of c-Myc, Fibronectin, Collagen I, and α-SMA in the indicated experimental groups. **(F)**Representative immunofluorescence images of Collagen I (red) in primary IPF fibroblasts. GFP indicates successfully transduced cells, and nuclei were counterstained with DAPI (blue). Scale bar: 100 μm. **(G)**Quantitative analysis of Collagen I-positive cells per field. Data are presented as mean ± SEM. Statistical significance was determined using Student's t-test (*$p < 0.05$, **$p < 0.01$, ***$p < 0.001$, ****$p < 0.0001$, ns = not significant).

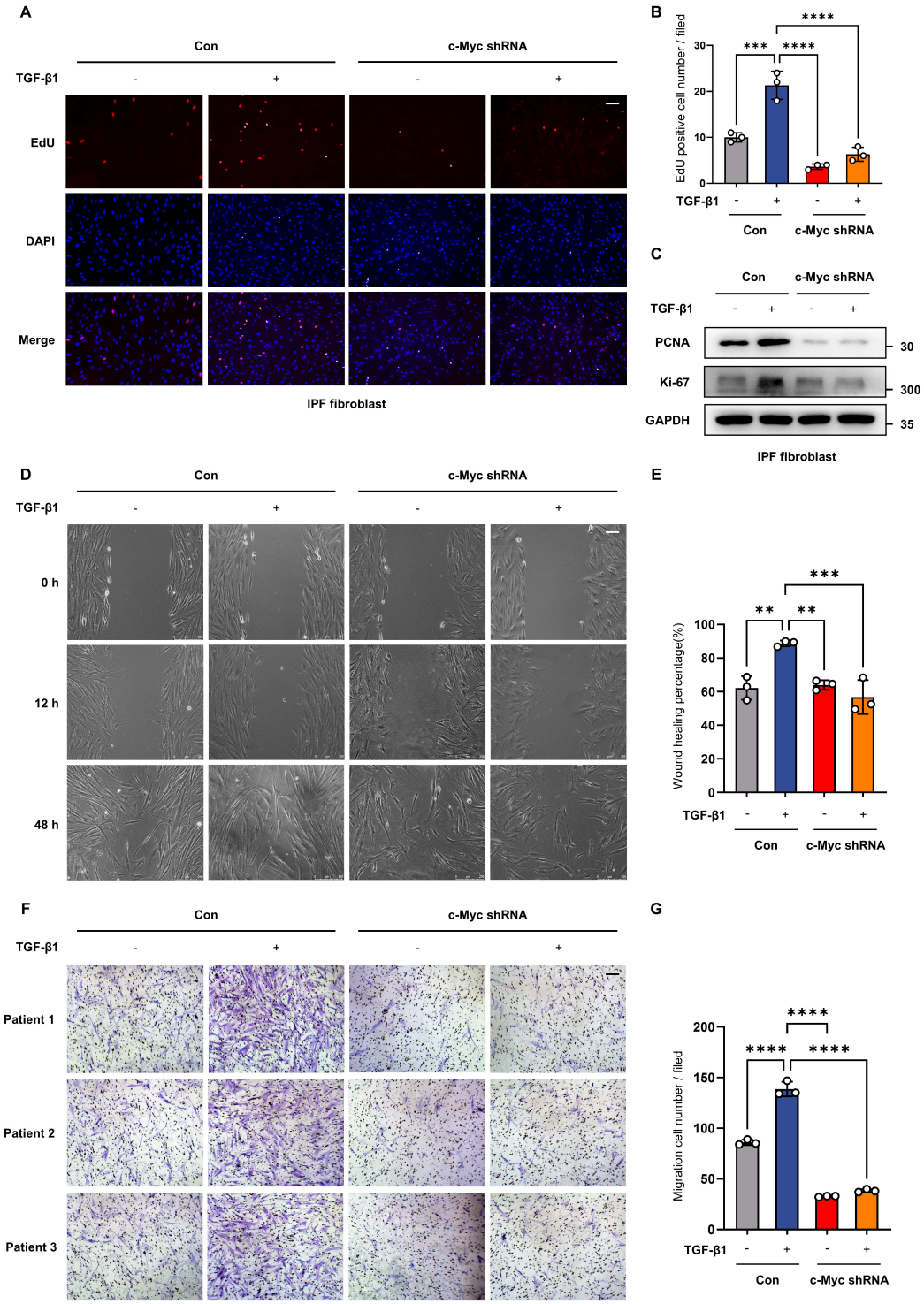


Figure 5

Impact of c-Myc knockdown on TGF-β1-induced proliferation and migration in primary IPF fibroblasts. **(A)**Representative fluorescence images of the EdU incorporation assay (EdU: red; DAPI: blue) in primary IPF fibroblasts transduced with control (Con) or c-Myc shRNA, in the presence or absence of TGF-β1 (10 ng/mL). Scale bar: 100 μm. **(B)**Quantitative analysis of EdU-positive cells per field. **(C)** Western blot analysis of cell proliferation markers PCNA and Ki-67 in the indicated experimental groups. GAPDH

served as the loading control. **(D and E)**Representative brightfield images of the wound-healing assay captured at 0, 12, and 48 h post-scratch (D), and corresponding quantification of the wound healing percentage at 48 h (E). Scale bar: 150 μm. **(F and G)**Representative images of transwell migration assays utilizing primary fibroblasts from three different IPF patients (Patient 1, Patient 2, and Patient 3) (F), and the corresponding quantification of migrating cells per field (G). Scale bar: 150 μm. Data are presented as mean ± SEM. Statistical significance was determined using Student's t-test (*p < 0.05, **p< 0.01, ***p < 0.001, ****p < 0.0001).

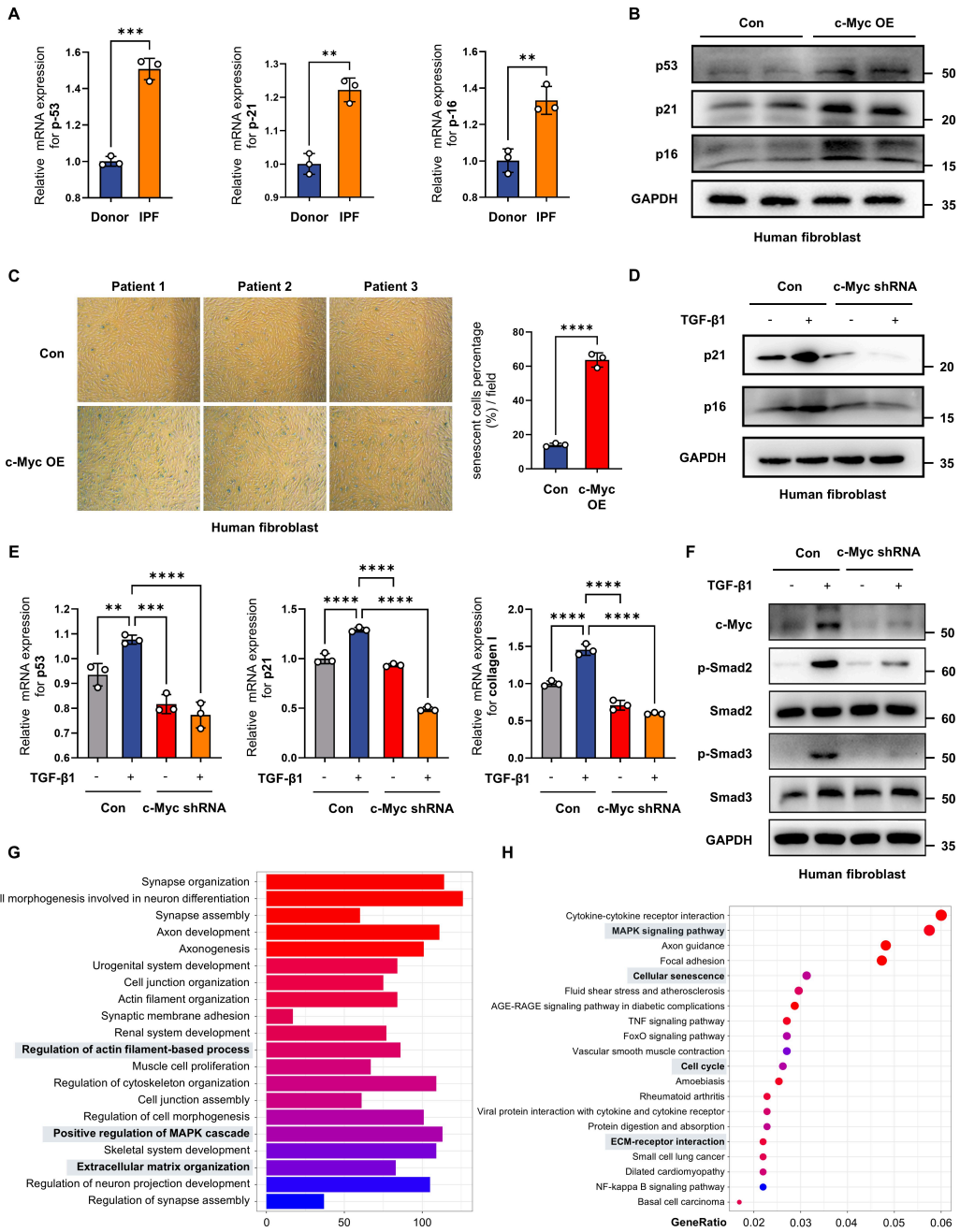


Figure 6

c-Myc promotes cellular senescence and regulates TGF-β1/Smad signaling in IPF fibroblasts. (A) RT-qPCR analysis of senescence markers p53, p21, and p16 in primary fibroblasts from healthy donors and IPF patients. **(B)** Western blot analysis of p53, p21, and p16 protein levels in control (Con) and c-Myc overexpressing (c-Myc OE) IPF fibroblasts. GAPDH served as the loading control. **(C)** Representative images and quantification of SA-β-gal staining in primary fibroblasts from three different IPF patients (Patient 1, Patient 2, and Patient 3) with or without c-Myc overexpression. **(D)** Western blot analysis of p21 and p16 in control and c-Myc shRNA-transduced IPF fibroblasts treated with or without TGF-β1 (10 ng/mL). **(E)** RT-qPCR analysis of p53, p21, and Collagen I mRNA expression in the indicated groups. **(F)** Western blot analysis of c-Myc, p-Smad2, Smad2, p-Smad3, and Smad3 in control and c-Myc knockdown IPF fibroblasts treated with or without TGF-β1. **(G and H)** Gene Ontology (GO) biological process (G) and KEGG pathway (H) enrichment analysis showing downregulated pathways in c-Myc shRNA fibroblasts compared to control fibroblasts under TGF-β1 treatment. Data are presented as mean ± SEM. Statistical significance was determined using Student's t-test (*$p < 0.05$, **$p < 0.01$, ***$p < 0.001$, ****$p < 0.0001$, ns = not significant).

Supplementary Files

This is a list of supplementary files associated with this preprint. Click to download.

- 20260702Supplement.docx
- 20260702Table.docx
- SFig.1.jpg
- SFig.2.jpg